Designing Organic Electron Transport Materials for Stable and Efficient Performance of Perovskite Solar Cells: A Theoretical Study

Aditya Kumar, Saurav Kumar Ojha, Nidhi Vyas, and Animesh K. Ojha*

Read Online

ACCESS | Metrics & More | Article Recommendations | SI Supporting Information

ABSTRACT: In this article, electron transporting layer (ETL) materials are designed to enhance the performance and stability of methyl ammonium lead iodide (MAPbI$_3$) perovskite solar cells (PSCs). The optical and electronic properties of the designed ETLs are investigated using density functional theory. The designed ETLs show better charge mobility compared to nickel phthalocyanines (NiPcs). The NiPc, a hole transporting layer material, shows ETL-like behavior for PSCs with the substitution of different electron withdrawing groups (X = F, Cl, Br, and I). The stability and electron injection behavior of the designed ETLs are improved. The Br$_{16}$NiPc shows the highest charge mobility. Further, the stability of the designed ETLs is relatively better compared to NiPc. Due to the hydrophobic nature, the designed ETLs act as a passivation layer for perovskites and prevent the absorber materials from degradation in the presence of moisture and provide extra stability to the PSCs. The effect of designed ETLs on the performance of MAPbI$_3$ solar cells is also investigated. The PSCs designed with Br$_{16}$NiPc as an ETL shows a relatively better (23.23%) power conversion efficiency (PCE) compared to a TiO$_2$-based device (21.55%).
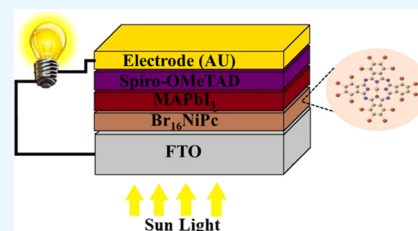
INTRODUCTION

In the recent decade, perovskite materials are considered as one of the alternatives for making solar cells (SCs) due to their cost effectiveness and efficiency.[1−4] In perovskite solar cells (PSCs), the perovskite material (ABX$_3$; A, B, and X are monovalent organic cations, divalent metal cations, and halogen ions, respectively[1]) is sandwiched between electron transport layers (ETLs) and hole transport layers (HTLs), which act as a light absorber.[4] The thermally generated electron−hole (e-h) pairs are transported to the photoanode and counter-electrode through ETLs and HTLs, respectively. Therefore, charge transport layers are the key components of PSCs as they work in the form of charge transportation, charge separation, and minimizing the rate of their recombination. Significant efforts were made to the design and synthesis of ETLs and HTLs with improved charge mobility to achieve better power conversion efficiency (PCE) of PSCs.[4−8] The materials containing small organic molecules are considered as a charge transport layer.[4−8] Generally, metal oxide, organic molecules, and polymers are used as ETLs for PSCs. TiO$_2$ material had widely been used as ETLs for PSCs.[5,9−11] The low electron mobility, high processing temperature, and a high density of trap states below the conduction band are the major key issues to make TiO$_2$ as a more reliable ETL. However, Snaith et al.[12] reported that TiO$_2$ reduces stability of PSCs. Further, the materials, e.g., SnO$_2$, CdSe, WO$_3$, ZnO, ZnSnO$_4$, and SrTiO$_3$ are also used as ETLs in PSCs.[13] Due to the low processing temperature, ZnO$_2$ reduces the effective cost of the PSC devices; however, low PCE, decomposition under ambient environment, and poor chemical stability of ZnO$_2$ are the main drawbacks before using it as ETLs. Further, SnO$_2$

is also used as an ETL in PSCs.[14] The charge mobility of SnO$_2$ is higher compared to TiO$_2$ and ZnO$_2$. The SnO$_2$ is less hygroscopic in nature compared to TiO$_2$ and ZnO$_2$; however, the devices with SnO$_2$ as an ETL are also reported to show poor PCE.[14]

Further, to overcome the shortcomings of oxide ETLs, one should have to search materials for better device stability and PCE. In this context, metal phthalocyanines (MPcs) may be a suitable candidate for ETLs in PSCs due to their unique properties, such as kinetic and thermal stability, considerable charge mobility, suitable band gap, and hydrophobicity in nature.[7] MPcs had been given a considerable attention due to their applications in organic solar cells and thin film transistors.[7] Most of the MPcs show an ideality factor, greater barrier height, and large series resistance. In a study,[15] the authors carried out density functional theory (DFT) calculations to explore the electronic structure and bonding in MPcs (M = Fe, Co, Ni, Cu, Zn, and Mg). Shah et al.[16] have investigated electrical properties of NiPc in a surface-type Schottky diode. Ahmad et al.[17] had studied the nickel(II) phthalocyanine-tetrasulfonic acid tetrasodium salt (NiTSPc) for its application as a temperature sensor. Further, a derivative of NiPc, nickel(II) 4,4′,4″,4‴ potassium-tetrasulfophthalocya-

nine (K$_4$NiTSPc) had also been investigated by Ahmad et al.[18] In the study, it was reported that the K$_4$NiTSPc shows better electronic properties compared to NiPc. Romero et al.[19] had investigated magnetic, electronic, and vibrational properties of MPcs (M = Ca, Sc, Ti, V, Cr, Mn, Fe, Co, Ni, Cu, Zn, and Ag) and fluorinated MPcs (F$_{16}$MPcs). Fadlallah et al.[20] had explored the electronic properties of F$_{16}$MPcs (M = Sc, Ti, V, Cr, Mn, Fe, Co, Ni, Cu, Zn, and Ag). Further, Haider et al.[21] had studied NiPc as an HTL for MA$_{0.21}$FA$_{0.78}$Pb (I$_{0.78}$Br$_{0.21}$)$_3$ PSCs and achieved a PCE of 14.3%.Generally, MPcs are p-type organic semiconductors; however, with the substitution of different electron extracting groups, e.g., −CN, −CF$_3$, halogens, and other functional groups, they behave like n-type semiconductors.[7,8,19,20] Further, there are some criteria for designing suitable ETL materials for PSCs, (i) the highest occupied molecular orbital (HOMO) level and lowest unoccupied molecular orbital (LUMO) level of ETLs must be lying below the HOMO and LUMO level of the corresponding perovskites, (ii) it must have high charge carrier mobility, (iii) electron affinity of ETLs should be high,[22] (iv) the recombination rate should be minimum, and (v) ETL materials should be chemically and kinetically stable.

By considering the above facts, we substituted halogens (X = F, Cl, Br, and I) as electron withdrawing functional groups in NiPc to modify its electronic properties and facilitate the designed molecules as n-type semiconductors that can be used as ETLs for PSCs. The structures, electronic and optical properties, and electron mobility of the functionalized NiPc molecules (XNiPc) with X = F$_{16}$, Cl$_{16}$, Br$_{16}$, and I$_{16}$ are studied using DFT. The optical absorption spectra of the designed ETL molecules are also studied using time-dependent DFT (TD-DFT). Further, the designed molecules are used as ETLs to simulate the efficiency of PSCs formed with the MAPbI$_3$ perovskite material as the light harvester via the SCAPS 1D solar cell simulator.[23]

COMPUTATIONAL METHODS

Theoretical Background. The Marcus theory[24,25] was employed to explore the charge transporting properties of the XNiPc molecule. Under ambient conditions, the hopping model is employed to describe the mobility of electrons and holes. The charge hopping rate (k) is defined as[24,25]

$$k = \frac{2\pi}{\hbar} V_{ab}^2 \frac{1}{\sqrt{4\pi\lambda k_B T}} \exp[-\lambda/4k_B T] \tag{1}$$

where V_{ab}, λ, $\hbar$, k_B, and T are the transfer integral, reorganization energy, Planck's constant, Boltzmann's constant, and temperature, respectively.

The change in energy associated to geometry relaxation during the charge transfer is known as reorganization energy, and it is defined as[4,6,26]

$$\lambda_{\text{hole}} = [E^0(M^+) - E^0(M^0)] + [E^+(M^0) - E^+(M^+)] \tag{2}$$

$$\lambda_{\text{ele}} = [E^0(M^-) - E^0(M^0)] + [E^-(M^0) - E^-(M^-)] \tag{3}$$

where λ_{hole} and λ_{ele} are reorganization energies of the hole and electron, respectively. M^0, M^+, and M^- are the optimized geometries of the neutral molecule, cation, and anion, respectively. $E^0(M^0)$ is the ground state energy of the neutral molecule, whereas $E^0(M^+)$ and $E^0(M^-)$ are the single-point energy of their cationic and anionic geometries, respectively.

The value of electronic coupling depends on the arrangement of the molecule in a solid state.[4] Further, in order to achieve high charge mobility, the value of electronic coupling should be at the maximum and reorganization energy should be at the minimum.[4] The value of electronic coupling is determined using the following equation:[27,28]

$$V_{ab} = \langle \psi_{\text{HOMO/LUMO}}^{0,a} | F | \psi_{\text{HOMO/LUMO}}^{0,b} \rangle \tag{4}$$

where $\psi_{\text{HOMO}}^{0,a}$ and $\psi_{\text{HOMO}}^{0,b}$ are the HOMOs of the two adjacent molecules, a and b, while $\psi_{\text{LUMO}}^{0,a}$ and $\psi_{\text{LUMO}}^{0,b}$ are the LUMOs of the same molecules without the intermolecular interaction and F is the Fock operator.

The mobility of the charge carrier (μ) of the designed molecules is obtained using the Einstein equation:[29]

$$\mu = \frac{eD}{k_B T} \tag{5}$$

where D and e are the diffusion coefficient and unit charge, respectively. The diffusion constant is expressed as

$$D = \frac{1}{2d} \sum_i r_i^2 k_i p_i \tag{6}$$

where i is the given transfer pathway, r_i, p_i $\left(p_i = k_i/\sum_i k_i\right)$, and d are the distance between the centroid to the centroid for charge hopping, hopping probability for the ith pathway, and spatial dimensionality, respectively. The value of d is considered as 1 in the present work.[30,31]

Further, we employed the SCAPS 1D solar cell simulator[23] to simulate the performance of PSCs using designed ETLs. To simulate the performance of PSCs like a real-life counterpart, the following differential equations in 1D are applied:

Poisson equation:

$$\frac{d}{dx}\left(-\varepsilon(x)\frac{d\psi}{dx}\right) = q[p(x) - n(x) + N_d^+(x) - N_a^-(x) + p_t(x) - n_t(x)] \tag{7}$$

where ε, Ψ, q, p, n, N_d^+, N_a^+, p_t, and n_t are the permittivity, electron charge, free hole density, free electron density, ionized donor-like doping concentration, ionized acceptor-like doping concentration, trapped hole density, and trapped electron density, respectively.

Hole continuity equation:

$$\frac{dp_n}{dt} = G_p - \frac{p_n - p_{n0}}{\tau_p} - p_n\mu_p\frac{d\xi}{dx} - \mu_p\xi\frac{dp_n}{dx} + D_p\frac{d^2p_n}{dx^2} \tag{8}$$

Electron continuity equation:

$$\frac{dn_p}{dt} = G_n - \frac{n_p - n_{p0}}{\tau_n} + n_p\mu_n\frac{d\xi}{dx} + \mu_n\xi\frac{dn_p}{dx} + D_n\frac{d^2n_p}{dx^2} \tag{9}$$

where G, D, ξ, and μ are the generation rate, diffusion coefficient, electric field, and mobility of the charge carrier, respectively.

Computational Details. To study the charge transport properties of XNiPc, we have first optimized their structures at the minima of the potential energy surface (PES) using Gaussian 09 software.[32] We have employed the B3LYP functional[33,34] conjugated with the basis set 6-311+g(d)[35] for lighter atoms, such as H, C, N, F, O, and Cl, and effective core

potential (ECP) basis set LANL2DZ[36] for heavy atoms, such as Br, I, and Ni, to perform the calculations. The calculation of the vibrational frequency is also done at the same level of theory to confirm that the structures are optimized at the minima of the potential energy surface (PES). We performed single-point calculations with the B3LYP[33,34] functional and single-point TD-DFT calculations with the Coulomb-attenuating method (CAM-B3LYP) functional[37] and 6-311+g(d)[35] and LANL2DZ[36] basis set to simulate the UV−vis spectra of XNiPc. In order to see the effect of the solvent on the simulated ultraviolet−visible (UV−vis.) spectra, the calculations were also performed in dimethyl sulfoxide (DMSO) as a solvent using a conductor-like polarizable continuum model (CPCM).[38]

■ RESULTS AND DISCUSSION

Structures and Molecular Orbitals. The optimized structures of NiPc and XNiPc (designed ETLs) are shown in Figure 1. For validation of the theoretical methods used in the
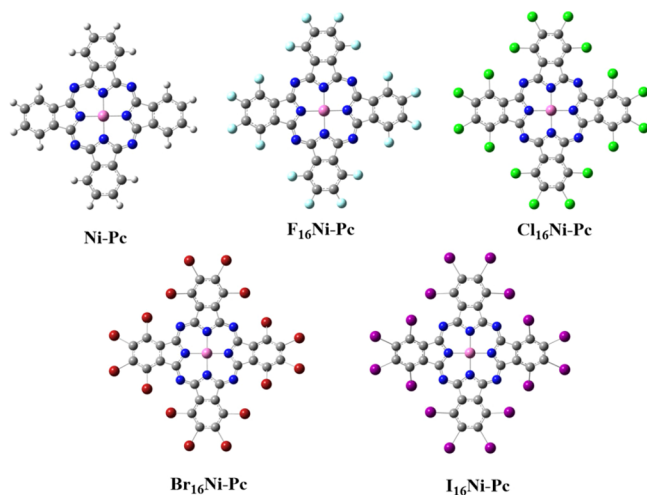

Figure 1. Optimized structures of NiPc and its derivative XNiPc.

present report, the calculated structural parameters of NiPc are compared with experimental data. The calculated results are given in the Supporting Information (SI), see Table S1. The molecular frontier orbitals of NiPc and XNiPc are calculated at the B3LYP/6-311+g(d)/LANL2DZ level of theory, and the results thus obtained are shown in Figure 2. The HOMOs and LUMOs of the designed molecules are mostly found to have a π character. It is important to note that in most of the
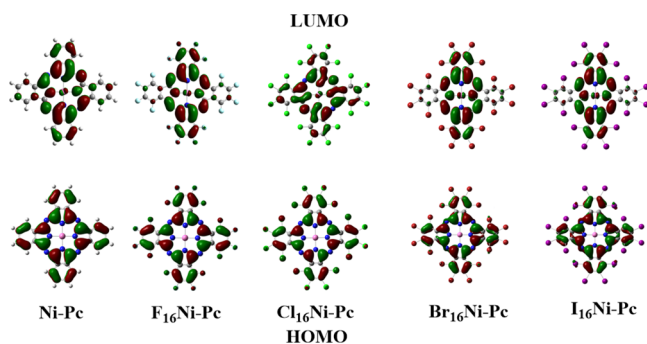

Figure 2. Calculated HOMO and LUMO levels of NiPc and its derivative XNiPc.

molecules, the HOMOs are more delocalized compared to LUMOs (see Figure 2). The delocalized frontier molecular orbitals, i.e., HOMO-LUMO orbitals can enhance the faster charge transportation by enhancing electronic coupling between adjacent molecules and reducing the nuclear reorganization energy. Further, the Ni atom mostly takes part in the formation of LUMOs. The HOMO of NiPc is calculated to be −5.26 eV. It is in good agreement with the previously reported value, −5.3 eV.[39] The substitution of electron withdrawing groups lowers the values of HOMOs and LUMOs compared with their values of NiPc. The value of the HOMO-LUMO gap is also decreased compared to NiPc. The calculated values of the HOMO-LUMO gap are shown in Table 1.

In Table 1, E_H, E_L, ΔE_{LH}, λ_{abs} (nm), E_{EX}, and f are the energy of the HOMO level, energy of the LUMO level, energy difference between HOMO and LUMO levels, maximum absorption wavelength, excitation energy for the lowest excited state that corresponds to the λ_{abs}, and oscillator strength of the lowest excitation, respectively.

To facilitate the electron mobility in the ETLs, the LUMO level must be lowered in case of n-type materials.[22] Further, the lower values of LUMOs contribute significantly to the environmental stability of the materials.[22,40,41] The LUMO levels of the designed ETL molecules can be regulated in the energy range −3.81 to −4.11 eV. Consequently, the value of HOMO and LUMO levels of MAPbI$_3$ is −5.43 and −3.93 eV, respectively. Thus, F$_{16}$Ni-Pc, Cl$_{16}$Ni-Pc, and Br$_{16}$Ni-Pc may be used as ETLs for MAPbI$_3$. However, the I$_{16}$Ni-Pc will not work as ETLs for MAPbI$_3$ since the HOMO and LUMO levels are not lying below the corresponding HOMO and LUMO levels of MAPbI$_3$ (see Table 1 and Figure 3). Therefore, we did not perform further calculations on I$_{16}$Ni-Pc as ETL for MAPbI$_3$, although it may work as ETL for another perovskite like MAGeI$_3$.

Electron Affinity, Ionization Potential, and Reorganization Energy. For n-type semiconducting materials, electron affinity (EA) must be higher to facilitate electron transport, whereas for p-type materials, ionization potential (IP) must be lower.[22] The values of IP and EA can be defined as IP = −E_{HOMO} and EA = −E_{LUMO}.[42] Due to substitution of different electron withdrawing groups to NiPc, the values of IP and EA are increased. This means that the electron mobility of XNiPc is enhanced compared to NiPc. The value of IP is found to be the maximum (6.24 eV) for F$_{16}$NiPc and the minimum (5.80 eV) for I$_{16}$NiPc. The value of EA is increased from 3.81 (I$_{16}$Ni-Pc) to 4.11 eV (F$_{16}$Ni-Pc). The calculated values of IP and EA are shown in Table 2. The values of EA of XNiPc are close enough to the work function of the most used metal electrode, e.g., gold with the work function 5.1 eV, which is being used in the present study[22] for simulating the efficiency of MAPbI$_3$.

The reorganization energy is a measure of change in energy associated with the geometry relaxation during the charge transfer. Further, according to Marcus, the low value of reorganization energy is required for better hopping of the charge carriers. The reorganization energies of the hole (λ_{hole}) are increased, while reorganization energies of the electron (λ_{ele}) are decreased for XNiPc (see Table 2). It further ensured that the XNiPc behaves as n-type semiconductors. The λ_{hole} and λ_{ele} for NiPc is calculated to be 0.04 and 0.33 eV, respectively. Further, the value of λ_{hole} and λ_{ele} is found in the range of 0.07−0.11 eV and 0.20−0.25 eV, respectively for

Table 1. Calculated Ground-State and Excited-State Properties of NiPc and its Derivatives

molecules	E_H (eV)	E_L (eV)	ΔE_{LH}(eV)	λ_{abs} (nm)	E_{EX} (eV)	f	assignment
Ni-Pc	−5.26	−3.06	2.20	649.13	1.91	0.66	H → L
F_{16}Ni-Pc	−6.24	−4.11	2.13	649.82	1.91	0.68	H → L
Cl_{16}Ni-Pc	−6.09	−4.00	2.09	660.94	1.88	0.70	H → L
Br_{16}Ni-Pc	−6.09	−4.01	2.08	684.58	1.81	0.76	H → L
I_{16}Ni-Pc	−5.80	−3.81	1.99	691.87	1.79	0.56	H → L
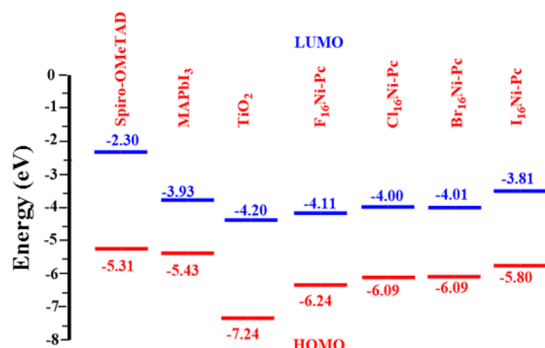
Figure 3. Band alignment of the HTL, perovskite, TiO_2, and designed ETLs.

Figure 4. UV−vis. spectra of NiPc and designed ETLs.

Table 2. Calculated Values of Reorganization Energy of Hole (λ_{hole}) and Electron (λ_{ele}), Ionization Potential (IP), Electron Affinity (EA), Exciton Binding Energy (E_B), and Amount of Charge Transfer (q_{CT}) of NiPc and XNiPc

molecules	λ_{hole} (eV)	λ_{ele} (eV)	IP (eV)	EA (eV)	E_B (eV)	q_{CT} (e) DMSO	q_{CT} (e) gas
Ni-Pc	0.04	0.33	5.26	3.06	0.29	0.34	0.26
F_{16}Ni-Pc	0.11	0.25	6.24	4.11	0.35	0.36	0.28
Cl_{16}Ni-Pc	0.10	0.25	6.09	4.00	0.27	0.39	0.32
Br_{16}Ni-Pc	0.08	0.22	6.09	4.01	0.27	0.38	0.31
I_{16}Ni-Pc	0.07	0.20	5.80	3.81	0.20	0.39	0.33

XNiPc. The lower value of λ_{ele} is better for improving the electron mobility of XNiPc. It further confirms that XNiPc may be used as ETLs for $MAPbI_3$.

Absorption Spectra, Exciton Binding Energy, and Charge Transfer. The ETLs must show less light absorption in the visible region besides the matching of the energy levels. To get insights into the optical properties and electronic transition of the designed ETLs, the UV−vis absorption spectra of the designed ETLs are calculated at the CAM-B3LYP/6-311+g(d)/LANL2DZ level of theory. The maximum absorption wavelength (λ_{abs}), oscillator strength (f), and excitation energy for the lowest excited state (E_{EX}) are listed in Table 1. The absorption spectra of the designed XNiPc molecules are shown in Figure 4. The simulated absorption peak of the designed ETLs shows significant absorption in the spectral range 649−692 nm. The Cl_{16}NiPc, Br_{16}NiPc, and I_{16}NiPc show a redshift of 12−43 nm compared to the absorption wavelength of NiPc. Kumar et al.[1] have calculated the absorption spectrum of $MAPbI_3$ with the absorption peak at 370 nm. The absorption range of ETLs is far from the absorption of $MAPbI_3$; therefore, the designed ETLs may be promising candidates for $MAPbI_3$. The maximum absorption of the designed ETLs is due to the electronic transition from HOMO to LUMO in the presence of large spatial overlapping of FMOs.
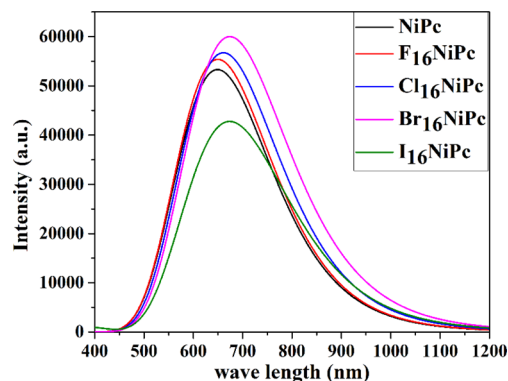
For effective charge transportation, the bound e-h pairs should be dissociated completely into negative and positive charges to avoid Coulomb attraction between them. The value of the exciton binding (E_B) energy is calculated by taking the energy difference of the electronic and optical band gap.[43] The first singlet excitation energy is considered as the optical band gap,[44] while the energy difference between HOMO and LUMO levels is approximated to the electronic band gap. The value of E_B of the designed ETLs ranges from 0.35 to 0.20 eV, while the E_B of the NiPc is calculated to be 0.29 eV. Except F_{16}NiPc, the values of E_B for other ETLs are found to be relatively less compared to NiPc (see Table 2). It shows that the e-h pairs of the designed ETLs, except F_{16}NiPc, can be dissociated into free charge carriers relatively easier compared to NiPc. Further, the amount of charge transfer (q_{CT}) in electronic transition also reflects the strength of the Coulomb attraction between e-h pairs.[4] The weak Coulombic attraction and faster dissociation of e-h pairs account for transfer of large amount of charge in electronic transitions.[4] To calculate the values of q_{CT}, we have employed the method reported by Ciofini et al.[45,46] The calculated values of q_{CT} in DMSO as a solvent and in the gas phase are shown in Table 2. The values of q_{CT} are calculated using Multiwfn software.[47] The value of q_{CT} for NiPc is calculated to be 0.34e and 0.26e in DMSO and the gas phase, respectively. The values of q_{CT} for designed ETL molecules are lying in the range of 0.36−0.39e and 0.28−0.33e in DMSO and the gas phase, respectively. The designed ETLs show a better charge transfer character compared to NiPc in electronic transitions. Therefore, an easy dissociation of e-h pairs can be expected in the designed ETLs due to large values of q_{CT} and the low value of E_B.

Charge Mobility. The charge mobility plays a key role in transporting the charge carriers; therefore, we have employed the Marcus[24,25] theory and the Einstein relationship[29] to obtain reliable charge mobility. For better charge mobility, the value of reorganization energy should be lower while the value of transfer integral should be larger. In earlier studies,[30,31] it was reported that the large value of the transfer integral results in the most stable dimer (the structures of the stable dimer of

designed ETLs are shown in the Supporting Information, see Figure S2). Therefore, herein, the charge transport pathways are considered only in one dimension instead of three dimensions. The values of electron mobility (μ_e), hole mobility (μ_h), centroid-to-centroid distances (r_i), electron transfer integral (V_{LL}), hole transfer integral (V_{HH}), and the hopping rate of electrons and holes are calculated for the stable dimer of the designed ETLs, and their values are listed in Table 3.

Table 3. Calculated Centroid-to-Centroid Distance (r_i), Hole Transfer Integral (V_{HH}), Electron Transfer Integral (V_{LL}), Hole Hopping Rate (k_h), Electron Hopping Rate (k_e), Hole Mobility (μ_h), and Electron Mobility (μ_e) of NiPc and XNiPc

molecules	r_i (Å)	V_{HH} (eV)	V_{LL} (eV)	k_h (s^{-1})	k_e (s^{-1})	μ_h (cm^2 V^{-1} s^{-1})	μ_e (cm^2 V^{-1} s^{-1})
Ni-Pc	5.43	3.91×10^{-3}	-1.34×10^{-3}	8.72×10^{11}	2.16×10^{9}	4.97×10^{-2}	1.23×10^{-4}
F$_{16}$Ni-Pc	3.95	1.02×10^{-2}	7.75×10^{-3}	1.82×10^{12}	1.80×10^{11}	5.49×10^{-2}	5.43×10^{-3}
Cl$_{16}$Ni-Pc	5.18	-1.97×10^{-3}	2.17×10^{-3}	2.11×10^{10}	2.56×10^{10}	1.09×10^{-3}	1.33×10^{-3}
Br$_{16}$Ni-Pc	4.86	1.53×10^{-1}	5.69×10^{-1}	6.42×10^{14}	1.38×10^{15}	29.30	62.99
I$_{16}$Ni-Pc	5.79	-3.75×10^{-2}	1.41×10^{-2}	4.54×10^{13}	1.08×10^{12}	2.94	6.99×10^{-2}

The designed ETL molecules, except Cl$_{16}$NiPc, show better values of μ_e and μ_h compared to NiPc. The values of μ_e and μ_h of Cl$_{16}$NiPc are found to be in the order of 10^{-3}, while for NiPc, the values of μ_e and μ_h are found to be in the order of 10^{-4} and 10^{-2}, respectively. The larger value of μ_h for NiPc compared to Cl$_{16}$NiPc may be due to the less value of V_{HH} and high value of λ_{hole} of Cl$_{16}$NiPc compared to their values of NiPc. Br$_{16}$NiPc shows the highest values of μ_e and μ_h among all the designed ETLs and NiPc. The shorter value of r_i and higher values of V_{LL} and V_{HH} are mainly responsible for the highest charge mobility of Br$_{16}$NiPc. Thus, the designed ETLs, F$_{16}$NiPc, Cl$_{16}$NiPc, and Br$_{16}$NiPc may be used as potential candidates for MAPbI$_3$, while, I$_{16}$NiPc may work for MAGeI$_3$. Thus, the higher value of μ_e of the designed ETLs allows them to serve as efficient ETLs without extra doping. Further, it can increase the stability of the device and also simplify the device fabrication.

Solubility and Stability. For the fabrication of PSCs, the solubility and stability of the designed ETLs are important properties, which need to be investigated. The solubility of the designed ETLs can be calculated using solvation free energy (ΔG_{sol}). It is defined as the difference between the free energy of the molecule in the gas phase and free energy of the molecule in the solution phase.[48] A high negative value of solvation energy of a molecule indicates its better solubility in the solution. In this work, we have calculated the solubility of the designed ETLs in two different solvents: (i) DMSO and (ii) dichloromethane (DCM). Further, the calculated results show that the designed ETLs have better solubility in DMSO in comparison to DCM, expect Cl$_{16}$NiPc, which shows better solubility in DCM (see Table 4). The better solubility of the designed ETLs will facilitate easy fabrication of the efficient PSCs.

Table 4. The Calculated Values of Solubility in DMSO and DCM, Chemical Hardness, Dipole Moment of NiPc and XNiPc

molecules	solubility (kcal/mol)		η (eV)	dipole moment (Debye)
	DMSO	DCM		
Ni-Pc	−7.93	−7.11	1.10	0.0004
F$_{16}$Ni-Pc	−14.43	−12.84	1.07	0.0005
Cl$_{16}$Ni-Pc	−8.07	−9.08	1.05	0.0001
Br$_{16}$Ni-Pc	−9.77	−8.71	1.04	0.1135
I$_{16}$Ni-Pc	−11.05	−9.92	1.00	0.0001

The stability of the designed ETL molecules is investigated by calculating the values of their chemical hardness (η).[42,49] The large value of η corresponds to higher stability of the ETLs. The value of η of the designed ETLs is calculated using the relation $(E_{LUMO} - E_{HOMO})/2$.[42] The calculated values of η are listed in Table 4. The values of η indicate that the stability of the designed ETLs is comparable to that of NiPc. Further, in order to use the designed ETLs as a passivation layer on the perovskites, we have also calculated their dipole moment. The values of the dipole moment of the designed ETLs are listed in Table 4. The values of dipole moment of the designed ETLs and NiPc are found to be nearly close to zero, expect Br$_{16}$NiPc. It shows the hydrophobic nature of the designed ETL molecules. Further, to check the hydrophobicity of the designed ETLs, we also studied the interaction of water with the designed ETL molecules. The calculated results are listed in Table 5.

Table 5. Calculated Values of the Bond Length of H−O of the Water Molecule Adsorbed on the Surface of NiPc and XNiPc

molecules	bond length (Å)	
	O−H(1)	O−H(2)
isolated H$_2$O molecule	0.963	0.963
Ni-Pc	0.964	0.964
F$_{16}$Ni-Pc	0.964	0.964
Cl$_{16}$Ni-Pc	0.964	0.964
Br$_{16}$Ni-Pc	0.964	0.964
I$_{16}$Ni-Pc	0.964	0.964

The results show that there is no deformation in the bond length (H−O) of the water molecule adsorbed on the surface of the designed ETLs. It further supports the hydrophobic nature of the designed ETLs. Therefore, the newly designed ETLs will act as the passivation layer on the surface of perovskites and prevent them to degrade in the open environment. Further, negligible structural changes are found in the designed ETLs due to adsorption of H$_2$O molecules (see Table S2 and Figures S3−S7).

Power Conversion Efficiency of Perovskite Solar Cells. In order to see the practical performance of designed ETL molecules, we have carried out numerical simulations via SCAPS-1D software[23] under the AM 1.5 solar spectrum at a 100 mW/cm^2 light intensity to determine J−V characteristics. The SCAPS-1D software describes thin film SCs as a stack of layers characterized by thickness, doping, and other physical parameters of the materials (absorber, ETL, and HTL)[50] as shown in Figure 5. The SC simulation software SCAPS-1D can simulate the electric field distribution, current density, recombination profile, and transport properties.[51,52] For the
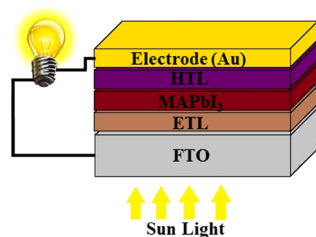
Figure 5. SCAPS−1D definition panel and device architecture (n−i−p).

reference SC device, we first simulate the solar cell using $MAPbI_3$ as the light absorber, TiO_2 as the ETL, and Spiro-OMeTAD as the HTL. The architecture of the device is considered to be a planar heterojunction n−i−p type as shown in Figure 5. Further, the energy level diagram used in SC simulation is listed in Figure 3. SC simulations are done at room temperature and under the AM 1.5 solar spectrum. The thickness of the absorber (perovskite), ETL, and HTL play an important role in deciding the performance of SCs. Therefore, we optimized the thickness of ETLs, while the thickness of the absorber and HTLs are taken from a previous work.[53] The optimized thickness of ETLs (TiO_2 for the reference device and designed ETLs) is listed in Table 6, and the variation of

Table 6. Optimized Thickness and Performance of PSC Devices with Different ETLs

ELT	thickness (nm)	V_{OC} (V)	J_{SC} (mA/cm^2)	FF (%)	PCE (%)
Spiro-OMeTAD as the HTL					
TiO_2	300	1.25	21.61	79.78	21.55
$Br_{16}NiPc$	300	1.254	22.62	81.92	23.23
$F_{16}NiPc$	300	1.24	17.14	81.54	17.29
NiPc as the HTL					
TiO_2	300	1.25	21.62	83.84	22.65
$Br_{16}NiPc$	300	1.25	22.62	85.13	24.14
$F_{16}NiPc$	300	1.24	17.14	85.06	18.04

PCE with ETL thickness and all the parameters of the absorber, ETLs, HTLs, and fluorine-doped tin oxide (FTO) are listed in the Supporting Information (see Table S3 and Figures S8−S18). Further, we use Spiro-OMeTAD and NiPc as HTLs to simulate the PCE of the SC devices. The optimized thickness of NiPc is found to be 300 nm. The optimized thickness of TiO_2, $Br_{16}NiPc$, and $F_{16}NiPc$ is found to be 300, 300, and 300 nm, respectively. The device parameters like open circuit voltage (V_{OC}), fill factor (FF), short circuit current (J_{SC}), and PCE of the SC devices are listed in Table 6. Considering Spiro-OMeTAD as the HTL, the TiO_2-based device shows a PCE of 21.55%, while the device based on $Br_{16}NiPc$ as ETLs shows a PCE of 23.23%. The I−V curve of the $Br_{16}NiPc$-based device is shown in Figure 6. Due to the small value of μ_h for $Cl_{16}NiPc$ ($\sim 10^{-3}$ cm^2 V^{-1} s^{-1}), we are not able to simulate the performance of the solar cell device with $Cl_{16}NiPc$ as ETLs. Thus, based on the above results, we can say that the use of $Br_{16}NiPc$ as an ETL provides enhanced PCE of the PSC device and with better stability in the presence of moisture.
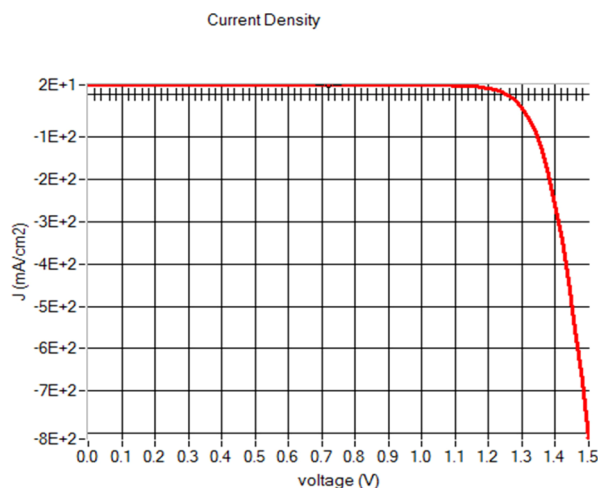

Figure 6. I−V graph and optimized performance of Br16NiPc as the ETL with a thickness of 200 nm and Spiro-OMeTAD as the HTL.

CONCLUSIONS

In this article, we have designed and studied ETLs for PSCs by substituting electron withdrawing groups (X = Fl, Cl, Br, and I) in NiPc. The addition of electron withdrawing groups modifies the electronic and optical properties of the NiPc. The stability of designed ETLs is found to be relatively better compared to NiPc. The designed ETLs show a better electron and hole hopping rate and electron and hole mobility compared to NiPc. The charge transfer characteristic is also enhanced in the designed ETLs. The designed ETLs show better solubility in DMSO compared to DCM. The designed ETLs are hydrophobic in nature; therefore, they will provide extra stability to the PSC devices in an open environment. Finally, we also calculated the PCE of the PSC devices using newly designed ETLs. The device with $Br_{16}NiPc$ as the ETL shows a PCE of 23.23 and 24.14% with Spiro-OMeTAD and NiPc as HTLs, respectively. Thus, among the designed ETLs, $Br_{16}NiPc$ provides better stability and enhanced PCE of $MAPbI_3$-based PSCs.

ASSOCIATED CONTENT

Ⓢ Supporting Information

The Supporting Information is available free of charge at https://pubs.acs.org/doi/10.1021/acsomega.1c00062.

> Structural parameters of optimized NiPc and its derivatives before and after the adsorption of water molecules and different parameters used in solar cell simulation (PDF)

AUTHOR INFORMATION

Corresponding Author

    Animesh K. Ojha − *Department of Physics, Motilal Nehru National Institute of Technology Allahabad, Prayagraj 211004, India;* ⓘ orcid.org/0000-0002-9546-4814; Email: animesh@mnnit.ac.in, animesh198@gmail.com

Authors

    Aditya Kumar − *Department of Physics, Chhatrasal Govt. PG college, Panna 488001, India; Department of Physics, Motilal Nehru National Institute of Technology Allahabad, Prayagraj 211004, India*

Saurav Kumar Ojha − *Department of Physics, Motilal Nehru National Institute of Technology Allahabad, Prayagraj 211004, India*

Nidhi Vyas − *School of Biotechnology, Jawaharlal Nehru University, New Delhi 110067, India*

Complete contact information is available at:
https://pubs.acs.org/10.1021/acsomega.1c00062

Notes

The authors declare no competing financial interest.

■ REFERENCES

(1) Kumar, A.; Singh, A.; Ojha, A. K. Reshuffling of Electronic Environment by Introducing CH3NH2F+ as an Organic Cation for Enhanced Power Conversion Efficiency and Stability of the Designed Hybrid Organic-Inorganic Perovskite. *J. Phys. Chem. C* **2019**, *123*, 13385−13393.

(2) Kojima, A.; Teshima, K.; Shirai, Y.; Miyasaka, T. Organometal halide perovskites as visible-light sensitizers for photovoltaic cells. *J. Am. Chem. Soc.* **2009**, *131*, 6050−6051.

(3) Yang, W. S.; Noh, J. H.; Jeon, N. J.; Kim, Y. C.; Ryu, S.; Seo, J.; Seok, S. I. High-performance photovoltaic perovskite layers fabricated through intramolecular exchange. *Science* **2015**, *348*, 1234−1237.

(4) Xu, Y.-L.; Ding, W.-L.; Sun, Z.-Z. How to design more efficient hole-transporting materials for perovskite solar cells? Rational tailoring of the triphenylamine-based electron donor. *Nanoscale* **2018**, *10*, 20329−20338.

(5) Jiang, X.; Yu, Z.; Li, H.-B.; Zhao, Y.; Qu, J.; Lai, J.; Ma, W.; Wang, D.; Yang, X.; Sun, L. A solution-processable copper (II) phthalocyanine derivative as a dopant-free hole-transporting material for efficient and stable carbon counter electrode-based perovskite solar cells. *J. Mater. Chem. A* **2017**, *5*, 17862−17866.

(6) Deng, J.; Hu, W.; Shen, W.; Li, M.; He, R. Exploring the electrochemical properties of hole transporting materials from first-principles calculations: an efficient strategy to improve the performance of perovskite solar cells. *Phys. Chem. Chem. Phys.* **2019**, *21*, 1235−1241.

(7) Sahoo, S. R.; Sahu, S.; Sharma, S. Charge transport and prototypical optical absorptions in functionalized zinc phthalocyanine compounds: A density functional study. *J. Phys. Org. Chem.* **2018**, *31*, No. e3785.

(8) Raïssi, M.; Vignau, L.; Ratier, B. Enhancing the short-circuit current, efficiency of inverted organic solar cells using tetra sulfonic copper phthalocyanine (TS-CuPc) as electron transporting layer. *Org. Electron.* **2014**, *15*, 913−919.

(9) Kogo, A.; Sanehira, Y.; Numata, Y.; Ikegami, M.; Miyasaka, T. Amorphous Metal Oxide Blocking Layers for Highly Efficient Low-Temperature Brookite TiO2-Based Perovskite Solar Cells. *ACS Appl. Mater. Interfaces* **2018**, *10*, 2224−2229.

(10) Ke, W.; Fang, G.; Wang, J.; Qin, P.; Tao, H.; Lei, H.; Liu, Q.; Dai, X.; Zhao, X. Perovskite Solar Cell with an Efficient TiO2 Compact Film. *ACS Appl. Mater. Interfaces* **2014**, *6*, 15959−15965.

(11) Lindblad, R.; Bi, D.; Park, B.-W.; Oscarsson, J.; Gorgoi, M.; Siegbahn, H.; Odelius, M.; Johansson, E. M. J.; Rensmo, H. Electronic Structure of TiO2/CH3NH3PbI3 Perovskite Solar Cell Interfaces. *J. Phys. Chem. Lett.* **2014**, *5*, 648−653.

(12) Leijtens, T.; Eperon, G. E.; Pathak, S.; Abate, A.; Lee, M. M.; Snaith, H. J. Overcoming ultraviolet light instability of sensitized TiO2 with meso-superstructured organometal tri-halide perovskite solar cells. *Nat. Commun.* **2013**, *4*, 2885.

(13) Mahmood, K.; Sarwar, S.; Mehran, M. T. Current status of electron transport layers in perovskite solar cells: materials and properties. *RSC Adv.* **2017**, *7*, 17044−17062.

(14) Noh, M. F. M.; Teh, C. H.; Daik, R.; Lim, E. L.; Yap, C. C.; Ibrahim, M. A.; Ludin, N. A.; bin Mohd Yusoff, A. R.; Jang, J.; Teridi, M. A. M. The architecture of the electron transport layer for a perovskite solar cell. *J. Mater. Chem. C* **2018**, *6*, 682−712.

(15) Liao, M.-S.; Scheiner, S. Electronic structure and bonding in metal phthalocyanines, metal= Fe, Co, Ni, Cu, Zn, Mg. *J. Chem. Phys.* **2001**, *114*, 9780−9791.

(16) Shah, M.; Sayyad, M. H.; Karimov, K. S.; Maroof-Tahir, M. Investigation of the electrical properties of a surface-type Al/NiPc/Ag Schottky diode using I−V and C−V characteristics. *Phys. B* **2010**, *405*, 1188−1192.

(17) Ahmad, Z.; Abdullah, S. M.; Sulaiman, K. Temperature-sensitive chemical cell based on Nickel (II) phthalocyanine-tetrasulfonic acid tetrasodium salt. *Sens. Actuators A* **2012**, *179*, 146−150.

(18) Ahmad, Z.; Sayyad, M. H.; Wahab, F.; Sulaiman, K.; Shahid, M.; Chaudry, J. A.; Munawar, M. A.; Aziz, F. Enhancement of electronic and charge transport properties of NiPc by potassium-tetrasulpho group. *Phys. B* **2013**, *413*, 21−23.

(19) Arillo-Flores, O. I.; Fadlallah, M. M.; Schuster, C.; Eckern, U.; Romero, A. H. Magnetic, electronic, and vibrational properties of metal and fluorinated metal phthalocyanines. *Phys. Rev. B* **2013**, *87*, 165115.

(20) Fadlallah, M. M.; Eckern, U.; Romero, A. H.; Schwingenschlögl, U. Electronic transport properties of (fluorinated) metal phthalocyanine. *New J. Phys.* **2016**, *18*, No. 013003.

(21) Haider, M.; Zhen, C.; Wu, T.; Wu, J.; Jia, C.; Liu, G.; Cheng, H.-M. Nickel phthalocyanine as an excellent hole-transport material in inverted planar perovskite solar cells. *Chem. Commun.* **2019**, *55*, 5343−5346.

(22) Chai, S.; Wen, S. H.; Huang, J. D.; Han, K. L. Density functional theory study on electron and hole transport properties of organic pentacene derivatives with electron-withdrawing substituent. *J. Comput. Chem.* **2011**, *32*, 3218−3225.

(23) Liu, F.; Zhu, J.; Wei, J.; Li, Y.; Lv, M.; Yang, S.; Zhang, B.; Yao, J.; Dai, S. Numerical simulation: toward the design of high-efficiency planar perovskite solar cells. *Appl. Phys. Lett.* **2014**, *104*, 253508.

(24) Marcus, R. A.; Sutin, N. Electron transfers in chemistry and biology. *Biochim. Biophys. Acta* **1985**, *811*, 265−322.

(25) Marcus, R. A. Electron transfer reactions in chemistry, Theory and experiment. *Rev. Mod. Phys.* **1993**, *65*, 599.

(26) Coropceanu, V.; Cornil, J.; da Silva Filho, D. A.; Olivier, Y.; Silbey, R.; Brédas, J.-L. Charge transport in organic semiconductors. *Chem. Rev.* **2007**, *107*, 926−952.

(27) Huang, J.; Kertesz, M. Intermolecular transfer integrals for organic molecular materials: can basis set convergence be achieved? *Chem. Phys. Lett.* **2004**, *390*, 110−115.

(28) Tang, X.-D.; Liao, Y.; Gao, H.-Z.; Geng, Y.; Su, Z.-M. Theoretical study of the bridging effect on the charge carrier transport properties of cyclooctatetrathiophene and its derivatives. *J. Mater. Chem.* **2012**, *22*, 6907−6918.

(29) Schein, L. B.; McGhie, A. R. Band-hopping mobility transition in naphthalene and deuterated naphthalene. *Phys. Rev. B* **1979**, *20*, 1631.

(30) Chi, W.-J.; Sun, P.-P.; Li, Z.-S. A strategy to improve the efficiency of hole transporting materials: introduction of a highly symmetrical core. *Nanoscale* **2016**, *8*, 17752−17756.

(31) Chi, W.-J.; Li, Q.-S.; Li, Z.-S. Exploring the electrochemical properties of hole transport materials with spiro-cores for efficient perovskite solar cells from first-principles. *Nanoscale* **2016**, *8*, 6146−6154.

(32) Frisch, M. J.; T, G. W.; Schlegel, H. B.; Scuseria, G. E.; Robb, M. A.; Cheeseman, J. R. et al. *Gaussian 09*, Revision C.01. Gaussian Inc. 2009.

(33) Becke, A. D. Density-functional thermochemistry. III. The role of exact exchange. *J. Chem. Phys.* **1993**, *98*, 5648−5652.

(34) Stephens, P. J.; Devlin, F. J.; Chabalowski, C. F.; Frisch, M. J. Ab Initio Calculation of Vibrational Absorption and Circular Dichroism Spectra Using Density Functional Force Fields. *J. Phys. Chem.* **1994**, *98*, 11623−11627.

(35) Krishnan, R.; Binkley, J. S.; Seeger, R.; Pople, J. A. Self-consistent molecular orbital methods. XX. A basis set for correlated wave functions. *J. Chem. Phys.* **1980**, *72*, 650−654.

(36) Chiodo, S.; Russo, N.; Sicilia, E. LANL2DZ basis sets recontracted in the framework of density functional theory. *J. Chem. Phys.* **2006**, *125*, 104107.

(37) Yanai, T.; Tew, D. P.; Handy, N. C. A new hybrid exchange−correlation functional using the Coulomb-attenuating method (CAM-B3LYP). *Chem. Phys. Lett.* **2004**, *393*, 51−57.

(38) Cossi, M.; Rega, N.; Scalmani, G.; Barone, V. Energies, structures, and electronic properties of molecules in solution with the C-PCM solvation model. *J. Comput. Chem.* **2003**, *24*, 669−681.

(39) Zhu, L.; Tang, H.; Harima, Y.; Kunugi, Y.; Yamashita, K.; Ohshita, J.; Kunai, A. A relationship between driving voltage and the highest occupied molecular orbital level of hole-transporting metal-lophthalocyanine layer for organic electroluminescence devices. *Thin Solid Films* **2001**, *396*, 214−219.

(40) Newman, C. R.; Frisbie, C. D.; da Silva Filho, D. A.; Brédas, J.-L.; Ewbank, P. C.; Mann, K. R. Introduction to organic thin film transistors and design of n-channel organic semiconductors. *Chem. Mater.* **2004**, *16*, 4436−4451.

(41) Fujisaki, Y.; Nakajima, Y.; Kumaki, D.; Yamamoto, T.; Tokito, S.; Kono, T.; Nishida, J.-I.; Yamashita, Y. Air-stable n-type organic thin-film transistor array and high gain complementary inverter on flexible substrate. *Appl. Phys. Lett.* **2010**, *97*, 133303.

(42) Kumar, A.; Singh, A.; Ojha, A. K. A new approach to predict the formation of 3D hybrid organic-inorganic perovskites. *Int. J. Quantum Chem.* **2019**, *119*, No. e26012.

(43) Scholes, G. D.; Rumbles, G. Excitons in nanoscale systems. In *Materials For Sustainable Energy: A Collection of Peer-Reviewed Research and Review Articles from Nature Publishing Group*, World Scientific: 2011; pp 12−25.

(44) Duan, Y. A.; Geng, Y.; Li, H. B.; Jin, J. L.; Wu, Y.; Su, Z. M. Theoretical characterization and design of small molecule donor material containing naphthodithiophene central unit for efficient organic solar cells. *J. Comput. Chem.* **2013**, *34*, 1611−1619.

(45) Ciofini, I.; Le Bahers, T.; Adamo, C.; Odobel, F.; Jacquemin, D. Through-space charge transfer in rod-like molecules: lessons from theory. *J. Phys. Chem. C* **2012**, *116*, 11946−11955.

(46) Le Bahers, T.; Adamo, C.; Ciofini, I. A qualitative index of spatial extent in charge-transfer excitations. *J. Chem. Theory Comput.* **2011**, *7*, 2498−2506.

(47) Lu, T.; Chen, F. Multiwfn: a multifunctional wavefunction analyzer. *J. Comput. Chem.* **2012**, *33*, 580−592.

(48) Ho, J.; Klamt, A.; Coote, M. L. Comment on the correct use of continuum solvent models. *J. Phys. Chem. A* **2010**, *114*, 13442−13444.

(49) Pearson, R. G. Absolute electronegativity and absolute hardness of Lewis acids and bases. *J. Am. Chem. Soc.* **1985**, *107*, 6801−6806.

(50) Decock, K.; Zabierowski, P.; Burgelman, M. Modeling metastabilities in chalcopyrite-based thin film solar cells. *J. Appl. Phys.* **2012**, *111*, No. 043703.

(51) Kanoun, A.-A.; Kanoun, M. B.; Merad, A. E.; Goumri-Said, S. Toward development of high-performance perovskite solar cells based on CH3NH3GeI3 using computational approach. *Sol. Energy* **2019**, *182*, 237−244.

(52) De Los Santos, I. M.; Cortina-Marrero, H. J.; Ruíz-Sánchez, M. A.; Hechavarría-Difur, L.; Sánchez-Rodríguez, F. J.; Courel, M.; Hu, H. Optimization of $CH_3NH_3PbI_3$ perovskite solar cells: A theoretical and experimental study. *Sol. Energy* **2020**, *199*, 198−205.

(53) Raoui, Y.; Ez-Zahraouy, H.; Tahiri, N.; El Bounagui, O.; Ahmad, S.; Kazim, S. Performance analysis of MAPbI3 based perovskite solar cells employing diverse charge selective contacts: Simulation study. *Sol. Energy* **2019**, *193*, 948−955.